Removal of Organic Films from Solid Surfaces Using Aqueous Solutions of Nonionic Surfactants. 2. Theory

Stephen P. Beaudoin, Christine S. Grant, and Ruben G. Carbonell*

Department of Chemical Engineering, North Carolina State University, Box 7905, Raleigh, North Carolina 27695

The removal of organic films of solder flux components (abietic acid in isopropyl alcohol) from disks of epoxy–glass laminate by aqueous solutions of nonionic surfactant ($C_{12}E_5$) proceeds through three stages. The controlling mechanisms in each stage were deduced from experimental observations. In this paper, theoretical models are developed to analyze the cleaning rates in the three different stages. The duration of the first stage is calculated assuming that convective and diffusive transport of surfactant monomer into the organic film controls the stage. The second stage is analyzed considering that shear forces remove aggregates from a continuous film of liquefied residue, while the third stage cleaning rate model is based on the shear-induced removal of isolated aggregates adsorbed directly to the solid substrate. Parameters in the models are evaluated using experimental cleaning rate data.

Introduction

In the previous paper, the mechanism by which a nonionic surfactant (pentaethylene glycol mono-*n*-dodecyl ether, $C_{12}E_5$) removed mixed films of abietic acid (AA) and isopropyl alcohol (IPA) containing up to 45% IPA from disks of FR-4 laminate was investigated using a rotating disk apparatus (Beaudoin et al., 1995). The cleaning experiments were conducted at 24 °C over a range of surfactant concentrations (4.1×10^{-3}, 1×10^{-3}, and 6×10^{-5} M $C_{12}E_5$), contaminant film thicknesses (1, 2, or 3 AA/IPA coats per disk), and disk rotational speeds (175, 350, 700, 1000, 1350, 1500, 1750, and 2000 rpm). Figure 1 is representative of the cleaning behavior observed in these experiments, and it shows clearly the existence of three different cleaning stages. Controlling mechanisms for the cleaning were proposed on the basis of the effects of the disk rotational speed, film thickness, and surfactant concentration on the cleaning rates.

In general, it was observed that the rate of cleaning in the first stage was low in comparison to that in the second stage. Experimental observations suggested that the first stage was controlled by penetration of surfactant into the AA/IPA film, transforming it from a solid to a liquid phase. The rate of cleaning observed in the second stage was the highest of the three stages. It was apparent that shear at the disk surface caused aggregates of liquefied film to be pulled from the surface during this stage. Finally, in the third stage, the cleaning rate was lower than that during the second stage, and the fractional AA removal was seen to approach 100% at long times. Physical arguments suggested that this stage was controlled by the shear-driven removal of isolated aggregates bound directly to the FR-4 laminate.

Surfactant partitioning and contacting experiments were conducted to investigate the penetration of surfactant into the AA/IPA films and to aid in the interpretation of the cleaning data. The partitioning results showed that surfactant penetrates into the films until it reaches equilibrium with the surfactant monomer concentration in aqueous solution. In contacting experiments, $C_{12}E_5$ was observed to penetrate into crystals of AA/IPA films, causing the crystals to be liquefied. No solubilization of the AA/IPA into the stationary aqueous phase was observed in these experiments.

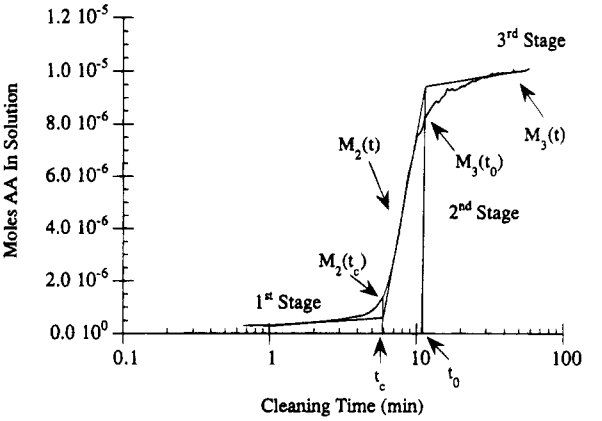

Figure 1. Observed cleaning stages: 4.1×10^{-3} M $C_{12}E_5$, 1750 rpm, disk with 3 AA/IPA coats, 24 °C.

The duration of the first stage decreased with increases in disk rotational speed and bulk surfactant concentration, but it increased with increases in the film thickness. The rate of the second stage was independent of the initial film thickness, although it increased with increases in the disk rotational speed and surfactant concentration. As in the second stage, the third stage cleaning rate increased with increases in the disk rotational speed and the surfactant concentration but was independent of the initial film thickness.

While many previous studies have described qualitatively the processes which occur during surfactant-based cleaning, there have been few attempts to describe mathematically the observed cleaning rates (Carroll, 1981, 1982; Shaeiwitz et al., 1981). In this paper, mass transport models for the different observed cleaning stages are developed and discussed. The cleaning data is analyzed using the models for each of the three stages. The excellent agreement found provides verification of the controlling mechanisms previously deduced from empirical observations.

Model Development and Results

First Stage Cleaning. The main process occurring during the first stage seems to be the penetration of

* Author to whom correspondence should be addressed. E-mail: ruben@ncsu.edu. Fax: (919) 515-3465.

0888-5885/95/2634-3318$09.00/0

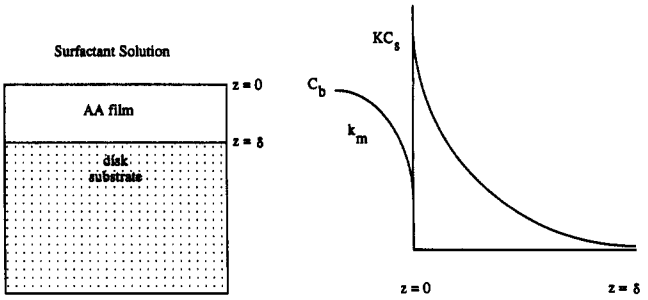

Figure 2. Penetration of $C_{12}E_5$ into AA/IPA films during first stage cleaning.

surfactant into the AA film, resulting in a liquefied film that is removed during the second and third stages. A schematic of the expected concentration profile of $C_{12}E_5$ in the AA/IPA film is presented in Figure 2. As the surfactant penetrates into the film, its concentration increases, film liquefaction occurs, and the viscosity of the film decreases to the point where hydrodynamic forces may remove aggregates of the film from the surface during the second stage. If this is correct, it is likely that a critical average concentration of surfactant within the film is required for the transition to the second cleaning stage to occur. The focus of the modeling effort was to relate the critical time at the end of the first stage, t_c, to the average surfactant concentration in the film. Figure 1 shows how t_c marks the transition from the low cleaning rate in the first stage to the fast cleaning observed in the second stage. It is understood that many parameters will affect t_c, including the rate of transport of surfactant from the bulk solution to the film surface, the rate of penetration of surfactant into the AA film, the rate of liquefaction of the film after surfactant penetration, the thickness of the film, the surfactant concentration in solution, and the shear stress at the film surface.

In modeling the first cleaning stage, it was assumed that the rate of penetration of surfactant into the film and the rate of transport of surfactant from the bulk solution to the film surface were controlling. As a first approximation, surfactant monomers were assumed to be transported to the film surface by convection, and the penetration of monomers into the film was assumed to occur by Fickian diffusion. On the basis of experimental observations, it was also assumed that the surfactant did not penetrate into the FR-4 laminate at the base of the organic layer. To model the penetration of surfactant into the films, experimental values of the film thickness, δ, were required for each film studied. Values of δ were calculated based on the mass of film present on the disks, the area of the disks, the film composition, and the density of the components in the films (AA and IPA). From buoyancy experiments conducted in sucrose solutions of known density, the density of AA was determined to be 1.07 g/cm^3. The calculated film thicknesses ranged from 10 μm in the films made from one AA/IPA coating to 35 μm for the films with three AA/IPA coatings. The rate of monomer adsorption at the interface was assumed to be fast compared to the rates of convective transport and diffusive penetration. As a result, the surfactant concentration at the interface in the film was assumed to be in equilibrium with the interfacial monomer concentration in solution. In the previous paper, experiments to determine the value of K, the equilibrium constant for the partitioning of surfactant monomer between the AA/IPA films and aqueous solution, were described (Beaudoin et al., 1995). Since the partitioning exhibited nonideal behavior, the values of the equilibrium constant were determined at the surfactant concentrations of interest (4.1×10^{-3}, 1×10^{-3}, and 6×10^{-5} M) by taking the ratio of the equilibrium concentrations of $C_{12}E_5$ monomer in the film and the bulk solution (found in Figure 3; Beaudoin et al., 1995). For the three surfactant concentrations studied here the values of K were approximately 11 100 (6×10^{-5} M) and 10 500 (4.1×10^{-3} and 1×10^{-3} M). For the two surfactant concentrations above the critical micelle concentration (cmc), the concentration of monomer in the bulk was considered to be the same as the cmc (6.4×10^{-5} M).

As a first approximation, it was assumed that micelles do not affect the rate of surfactant penetration into the AA/IPA films. As a result, differences between model predictions and experimental data on the effect of surfactant concentration on t_c can be ascribed to the role of micelles in the first stage. Also, it was assumed that the value of t_c for each experiment was not affected by the level of shear stress at the film surface. The validity of this assumption can be tested by analyzing experimental data on the effect of rotational speed on t_c. The value of the molecular diffusion coefficient for the $C_{12}E_5$ monomer in the AA/IPA film, D_{SA}, was not known *a priori*. This parameter was very difficult to measure experimentally, so its value was estimated based on comparisons of the model and the experimental data (see below).

Given these assumptions, the diffusion equation for monomer in the film is given by

$$\frac{\partial C}{\partial t} = D_{SA}\frac{\partial^2 C}{\partial z^2} \tag{1}$$

subject to

$$t = 0: \quad C = 0$$

$$z = 0: \quad -D_{SA}\frac{\partial C}{\partial z} = k_m[C_b - C_S]; \quad C = KC_S$$

$$z = \delta: \quad \frac{\partial C}{\partial z} = 0$$

where C = concentration of $C_{12}E_5$ in AA/IPA film [M], D_{SA} = diffusion coefficient of $C_{12}E_5$ in AA/IPA film [cm^2/s], K = equilibrium constant for $C_{12}E_5$ absorption into AA/IPA film, k_m = mass transfer coefficient for transport of $C_{12}E_5$ monomer from bulk solution to disk surface [cm/s], C_S = interfacial concentration of $C_{12}E_5$ in solution [M], and C_b = bulk concentration of $C_{12}E_5$ monomer in solution [M]. The first boundary condition takes into account the effect of convective transport of surfactant monomer to the film surface. The value of k_m was calculated using the expression for the mass transfer coefficient for a rotating disk under laminar flow conditions (Cochran, 1934; Levich, 1942),

$$k_m = 0.6205\nu^{-1/6}D^{2/3}\omega^{1/2} \tag{2}$$

where k_m = mass transfer coefficient in fluid phase [cm/s], ν = fluid kinematic viscosity [cm^2/s], D = diffusion coefficient for $C_{12}E_5$ monomer in solution [cm^2/s], and ω = rotational speed of disk [rad/s].

D in eq 2 was calculated to be 4.0×10^{-6} cm^2/s from the Stokes–Einstein equation (Geankoplis, 1983). This calculation required evaluation of the molar volume of $C_{12}E_5$ monomer at its normal boiling point, and this

parameter was estimated by summing the atomic volumes of the C, H, and O atoms in the $C_{12}E_5$ molecule, to give a value of 570 cm^3/mol (Geankoplis, 1983).

Equation 1 may be nondimensionalized as follows

$$\frac{\partial U}{\partial \Theta} = \frac{\partial^2 U}{\partial X^2} \tag{3}$$

subject to

$$\Theta = 0: \quad U = 0$$

$$X = 0: \quad \frac{\partial U}{\partial X} = Bi(1 - U)$$

$$X = 1: \frac{\partial U}{\partial X} = 0$$

where $\Theta = tD_{SA}/\delta^2$, $U = C/(KC_b)$, $X = z/\delta$, and $Bi = k_m\delta/(D_{SA}K)$ = mass transfer Biot number [dimensionless]. The solution to eq 3 was obtained by separation of variables resulting in

$$U = 1 - \sum_{n=1}^{\infty}[(\tan(\alpha_n)\sin(X\alpha_n) + \cos(X\alpha_n)) \times \tan(\alpha_n)\exp[-\alpha_n{}^2\Theta]]/\left[\alpha_n \tan^2(\alpha_n)\left(\frac{1}{2} - \frac{\sin(2\alpha_n)}{4\alpha_n}\right) - \sin(\alpha_n)\cos(\alpha_n) + \tan(\alpha_n) + \frac{\alpha_n}{2} + \frac{\sin(2\alpha_n)}{4}\right] \tag{4}$$

where α_n are eigenvalues obtained from

$$Bi = \alpha_n \tan(\alpha_n) \tag{5}$$

The eigenvalues for each value of Bi were calculated iteratively and were checked using values from the literature (Abramowitz and Segun, 1968). The first nine eigenvalues were used in computations, although for the range of parameter values of interest, the solution was only sensitive to the first three eigenvalues. The dimensionless saturation of surfactant in the AA/IPA film, U, can be averaged over the film thickness

$$\langle U\rangle = \frac{\langle C\rangle}{KC_b} = \int_0^1 U\,dX \tag{6}$$

Integration of eq 4 results in an expression for the average surfactant saturation in the organic film

$$\langle U\rangle = 1 - \sum_{n=1}^{\infty}(\tan^2(\alpha_n)\exp[-\alpha_n{}^2\Theta])/\left[\alpha_n{}^2\tan^2(\alpha_n)\left(\frac{1}{2} - \frac{\sin(2\alpha_n)}{4\alpha_n}\right) + \alpha_n(\tan(\alpha_n) - \sin(\alpha_n)\cos(\alpha_n)) + \frac{\alpha_n{}^2}{2} + \frac{\alpha_n\sin(2\alpha_n)}{4}\right] \tag{7}$$

Using eqs 5 and 7, it is possible to generate curves of the critical dimensionless time Θ_c required, at a given value of Bi, to reach a given value of the average surfactant saturation $\langle U\rangle$ in the film. Experimental values of Θ_c corresponding to the end of the first stage were calculated using experimental values of the film thickness δ, the time when the first stage ended t_c, and an estimated D_{SA} value of 2.7 × 10^{-9} cm^2/s (discussed below). As indicated in Figure 1, t_c was calculated by drawing tangents to the linear portions of the first and second cleaning stages. The time value at the intersection of these tangents was t_c. Using experimentally measured values of δ and K, calculating the value of k_m from eq 2, and using the estimated D_{SA} values, experimental values of Bi were computed. This allowed for a comparison between the experimental and theoretical values of Θ_c for the range of possible values of $\langle U\rangle$ from 0 to 1.

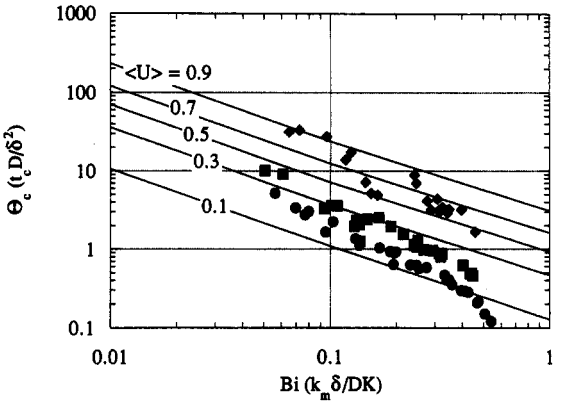

Figure 3. First stage cleaning comparison, theory and experiment: 24 °C, D_{SA} = 2.7 × 10^{-9} cm^2/s (◆, 6 × 10^{-5} M $C_{12}E_5$, 1500–175 rpm, 1, 2, and 3 AA/IPA coats; ■, 1 × 10^{-3} M $C_{12}E_5$, 1500–175 rpm, 1, 2, and 3 AA/IPA coats; ●, l: 4.1 × 10^{-3} M $C_{12}E_5$, 1500–175 rpm, 1, 2, and 3 AA/IPA coats).

A comparison between experimental and theoretical values of Θ_c is shown in Figure 3. Data for disks with one, two, and three coatings of AA/IPA are included at three surfactant concentrations (4.1 × 10^{-3} M, 1.0 × 10^{-3} M, and 6 × 10^{-5} M). Within each data set, the points with the smallest values of Bi correspond to the disks with one coating (smallest δ), the intermediate Bi values belong to the disks with two coatings (intermediate δ), and the highest Bi values are for the disks with three coatings (largest δ).

To calculate the value of D_{SA}, it was assumed that the fractional saturation of the film $\langle U\rangle$ at t_c was equal to 0.15 for the 4.1 × 10^{-3} M data, while for the 6 × 10^{-5} M case, $\langle U\rangle$ was assumed to equal 0.7. Values of D_{SA} were then assumed and the experimental values of Bi and Θ_c were calculated as discussed above. Using this computed Bi and the assumed value of $\langle U\rangle$, eqs 5 and 7 were used to calculate a theoretical value of Θ_c, which was compared to the experimental value. The values of D_{SA} which gave the least squared normalized deviations between the experimental and theoretical values of Θ_c were 2.8 × 10^{-9} cm^2/s for the 6 × 10^{-5} M data and 2.6 × 10^{-9} cm^2/s for the 4.1 × 10^{-3} M data. A mean value of 2.7 × 10^{-9} cm^2/s was taken for D_{SA} and used to generate the results shown in Figure 3.

As can be seen in Figure 3, the data are bracketed by physically-meaningful values of the surfactant saturation of the film $\langle U\rangle$. It also can be seen that the effect of the film thickness on the duration of the first stage has been successfully addressed by this model, as the experimental data for three film thicknesses collapse onto the same curve for each surfactant concentration considered. However, there is a difference between the slopes of the theoretical and experimental curves. The experimental data for Θ_c exhibits a stronger dependence on Bi than the model. This is probably due to the effect of shear stress on the transition from the first to the second stage (t_c). At high values of Bi, the disk

rotational speed is high, and the shear stress at the surface of the disk is correspondingly high. Under these conditions, aggregates may be pulled from more viscous films (lower surfactant saturation) than at low values of the shear stress, allowing the transition to the second stage to occur at a lower value of t_c than can be predicted from transport considerations only. The model that has been developed here estimates the surfactant concentration in the film at t_c based on the rate of convective transport of surfactant to the film surface, and it does not take into account any factors affecting t_c except the rate of surfactant penetration into the organic film. Since the relationship between shear stress and the duration of the first stage is not taken into account, the model overpredicts the amount of surfactant required in the film at high shear stress values, so that the slopes are slightly different between the theory and experiment.

It also is apparent in Figure 3 that the critical time data for the three different surfactant concentrations fall on three nearly parallel lines, rather than collapsing onto one line. This effect is probably due to the effect of the presence of micelles on t_c. As discussed in the previous paper, micelles in solution can decrease the duration of the first stage (lower value of t_c) by increasing the driving force for surfactant penetration into the AA films or by facilitating the dissolution of aggregates into the cleaning solution (Beaudoin et al., 1995). If one micelle adsorbs to the interface and dissociates, it can liberate many surfactant monomers in the interfacial zone, greatly enhancing the driving force for surfactant penetration into the films compared to the case of monomer transport only. Alternatively, as the surface of the organic film becomes more liquid-like, micelles may enhance the rate of film dissolution, hastening the transition to the second stage. Neither of these possible effects are considered in the model, although both would cause a reduction in the experimental value of t_c at a given value of Bi. This reduction would be expected to be proportional to the concentration of micelles in the system, with higher micellar concentrations producing larger reductions in t_c. The presence of three parallel lines shown by the experimental data in Figure 3 is consistent with these effects.

The residence time of surfactant solution in the analytical loop of the experimental apparatus was approximately 1 min. In experiments where the duration of the first stage was very short (from 6 to 10 min; 4.1×10^{-3} M, 1000−1500 rpm; 1×10^{-3} M, 1500 rpm), it was expected that the time required to detect changes in the AA content of the cleaning solution would begin to be slow compared to the cleaning rate at these conditions, resulting in measured t_c values higher than expected. In fact, Figure 3 shows that the values of t_c for the 4.1×10^{-3} and 1×10^{-3} M data follow a very uniform trend, and there is no evidence that this effect influenced the data. This suggests that due to the low cleaning rate during the first stage, the residence time in the experimental loop did not significantly affect the monitoring of the experiments.

In summary, the simple model presented here, based on Fickian diffusion of surfactant monomer into the AA/IPA films, suggests that there is a correlation between the fractional surfactant saturation of the organic film and the time required for the transition from the first to the second stage of cleaning. The model correctly addresses the effect of the initial film thickness on the duration of the first stage. The model does not account for the effect of micelles or shear stress on the duration of the first stage, but the calculations shown here help to demonstrate the importance of these effects.

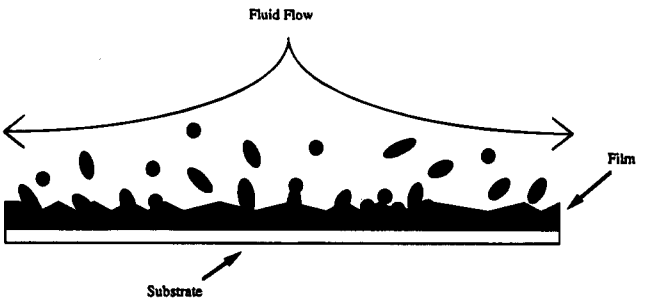

Figure 4. Second stage cleaning mechanism.

Second Stage Cleaning. The second stage was modeled by assuming that surfactant-laden aggregates of AA are sheared from a continuous film of liquefied AA. The shear at the disk surface is created when cleaning fluid flows radially outward across the film surface due to the rotation of the disk, and this shear causes aggregates to form and be removed from the surface of the liquefied AA. This is represented schematically in Figure 4. It is expected that the rate of cleaning observed during the second stage should be independent of the amount of AA present on the disk, as long as the film remains continuous.

To model the second stage cleaning, the rate of aggregate removal was related to a kinetic constant that was assumed to depend on the shear stress at the disk surface. The constant was taken to be independent of the mass of AA on the disk but was expected to vary with surfactant concentration, since it was shown in the previous paper that the second stage cleaning rate is an increasing function of surfactant concentration (Beaudoin et al., 1995). With these assumptions, the rate of cleaning in the second stage may be expressed in the form

$$\frac{dM_2}{dt} = k = \beta\overline{\tau_{rz}} \qquad t_c < t < t_0 \tag{8}$$

where M_2 = moles AA in solution during second stage, k = aggregate desorption rate constant [mol/min], β = proportionality constant [mol/stress time], and $\overline{\tau_{rz}}$ = radially-averaged shear stress at film surface [g/cm·s^2]. This equation is valid in the range of time from t_c to t_0, as shown in Figure 1. It is expected that β will vary with the surfactant concentration in solution and be independent of film thickness, consistent with the effects of surfactant concentration and film thickness on the second stage cleaning. The shear stress on the surface of the disk is given by the expression (Middleman, 1987; Strong and Middleman, 1989)

$$\tau_{rz} = 0.51\mu r\nu^{-1/2}\omega^{3/2} \tag{9}$$

where τ_{rz} = shear stress on the disk surface [g/cm·s^2], μ = fluid viscosity [g/cm·s], ω = disk rotational speed [rad/s], r = radial position on disk surface [cm], and ν = kinematic viscosity of fluid [cm^2/s]. Averaging eq 9 over the area of the disk, it is possible to determine the mean shear stress on the disk surface

$$\overline{\tau_{rz}} = \frac{2R}{3}0.51\mu\nu^{-1/2}\omega^{3/2} \tag{10}$$

By combining eq 8 and 10, the relationship between the

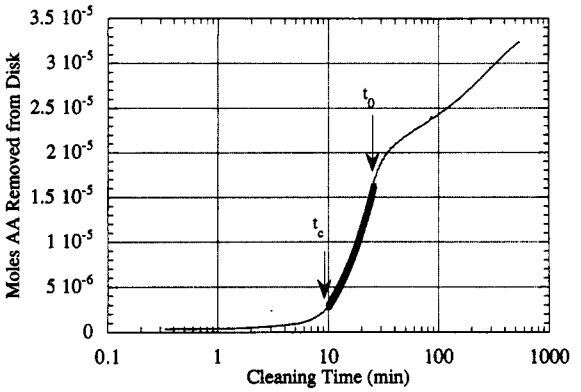

Figure 5. Second stage: typical agreement, theory and experiment.

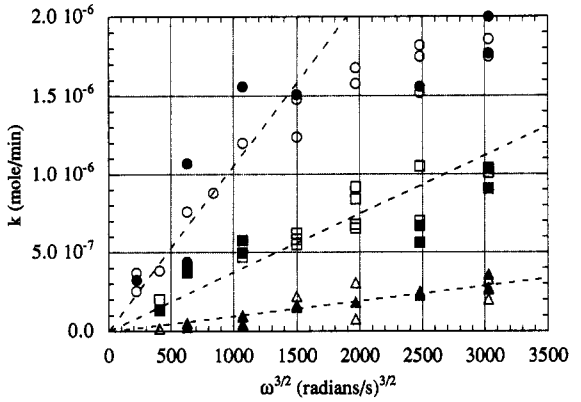

Figure 6. Evaluation of shear-controlled cleaning during second cleaning stage: disks with 1 (hollow symbols) and 3 (filled symbols) AA/IPA coats, 24 °C (○, ●, 4.1×10^{-3} M $C_{12}E_5$; □, ■, 1×10^{-3} M $C_{12}E_5$; △, ▲, 6×10^{-5} M $C_{12}E_5$).

slope of the second stage cleaning data and the disk rotational speed becomes

$$\frac{dM_2}{dt} = k = \beta\frac{2R}{3}0.51\mu\nu^{-1/2}\omega^{3/2} \qquad (11)$$

The parameters μ and ν on the right-hand-side of eq 11 should be essentially constant for all experimental conditions considered here. However, β will vary with the surfactant concentration in solution, as discussed above. Experimental values of k were calculated from the slopes of the second stage cleaning curves (dM_2/dt), as shown in Figure 1. A typical fit of eq 11 to experiment is shown in Figure 5.

Plots of the slopes of the second stage cleaning data, k, against $\omega^{3/2}$ for each surfactant concentration considered should give straight lines that go to zero when the value of the rotational speed goes to zero, if the proposed mechanism is correct. These lines should be independent of the initial film thickness, as processes acting on the surface of the AA/IPA films should not be affected by the quantity of film below the surface. The lines also should vary with the surfactant concentration in solution, with higher surfactant concentrations providing higher values of k at all values of the shear stress.

Figure 6 presents the relationship between the slope of the second stage cleaning curves, k, and $\omega^{3/2}$ for disks with one and three coats of AA/IPA at 4.1×10^{-3}, 1×10^{-3}, and 6×10^{-5} M $C_{12}E_5$. As can be seen, there is a linear relationship between k and $\omega^{3/2}$ at low values of the shear stress ($\omega^{3/2}$) for all surfactant concentrations, and the value of the desorption constant goes to zero as the shear stress goes to zero. In addition, the values of

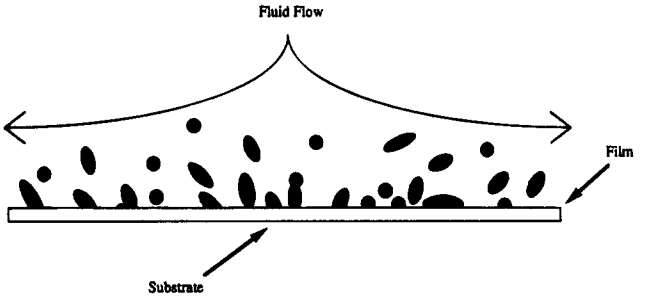

Figure 7. Third stage cleaning mechanism.

k for disks with one and three AA/IPA coats are essentially identical. Also, it can be seen that the slopes of the curves in Figure 6 increase with increasing surfactant concentration. As discussed in the previous paper, the rate of aggregate removal in the second stage is increased when the concentration of micelles in solution increases, as the micelles apparently facilitate the desorption of aggregates from the film surface (Beaudoin et al., 1995).

For the highest value of the surfactant concentration (4.1×10^{-3} M), at high values of the shear stress, it is seen in Figure 6 that the rate at which the desorption constant increases with increasing shear is somewhat diminished. For the lower surfactant concentrations, however, this effect is not observed. The change seen at high values of the shear stress in the 4.1×10^{-3} M case is probably an artifact of the experimental system. As mentioned above, the residence time of the surfactant solution in the analytical loop of the experimental apparatus is approximately 1 min. For the desorption constants in question, the duration of the second stage varies from approximately 4 to 12 min, depending on the disk rotational speed and the film thickness. Under these conditions, the rate at which changes in the AA content of the solution can be observed begins to be slow compared to the rate at which AA is removed from the disk surface, and the values of the calculated desorption constant are lower than expected. Only the systems with the fastest second stages (those with the highest shear rates and highest surfactant concentrations) show this effect. With the exception of a few data points at the high values of $\omega^{3/2}$ for the 4.1×10^{-3} M concentration, the agreement between the model expectations and the experimental data is excellent.

In summary, over a 2 order-of-magnitude change in surfactant concentration and a greater than 1 order-of-magnitude change in the value of $\omega^{3/2}$, the model accurately describes the cleaning data. The removal of aggregates during the second stage is seen to increase linearly with increases in the shear stress and is independent of the thickness of the film initially present on the disk, although it increases with increasing concentrations of surfactant in solution.

Third Stage Cleaning. It is assumed that at the end of the second stage, the continuous film of AA has been removed, leaving only "islands" of AA surrounded by bare substrate on the FR-4 laminate, as shown in Figure 7. As mentioned in the previous paper, when cleaning experiments were stopped during the third stage, such residual AA "islands" were observed on the FR-4 surface (Beaudoin et al., 1995). In this situation, the solution–AA interface is no longer continuous, and it is expected that the rate of cleaning will depend on the amount of AA remaining on the disk. However, the initial film thickness is not expected to affect the cleaning during the third stage, as processes occurring

at the AA–FR-4 interface should be independent of the thickness of film that was initially in place. Also, as observed in the previous paper, it is expected that the rate of aggregate desorption during the third stage will be increased with increasing concentrations of surfactant in the system, due to the ability of micelles to enhance aggregate desorption (Beaudoin et al., 1995).

To model the cleaning rate in the third stage, it was assumed that the aggregates ("islands") of AA on the FR-4 were pulled from the surface by shear forces. The rate of removal of aggregates of a given size was considered to be a first-order process in the number of aggregates of that size on the disk surface,

$$\frac{dN_i}{dt} = -\hat{k}_i N_i \qquad t_0 < t < \infty \tag{12}$$

where $\hat{k}_i$ = desorption rate constant for islands of characteristic size σ_i [1/time], N_i = number of aggregates of characteristic size σ_i, and t_0 = time at start of third stage [min]. The start of the third stage, t_0, and the moles of AA in solution at the start of the third stage, $M_3(t_0)$, are defined by the intersection of tangents drawn through the second and third stage cleaning data, as shown in Figure 1. It is possible to define the average number of aggregates on the disk surface by the relation

$$\bar{N} = \int_0^\infty N_i P(\sigma_i)\, d\sigma_i \tag{13}$$

where $P(\sigma_i)$ = normalized probability of finding an aggregate of size σ_i. By multiplying eq 12 by $P(\sigma_i)$ and integrating over all aggregate sizes, it is possible to determine the mean rate of aggregate removal

$$\frac{d\bar{N}}{dt} = -\int_0^\infty \hat{k}_i N_i P(\sigma_i)\, d\sigma_i \tag{14}$$

The right-hand side of eq 14 can be used to define a mean aggregate desorption constant, $\hat{k}$ (1/time), such that

$$\frac{d\bar{N}}{dt} = -\hat{k}\bar{N} \tag{15}$$

The number of moles of AA on the disk may be written in the form

$$\hat{M}_3 = \bar{M}\bar{N} \tag{16}$$

where $\hat{M}_3$ = moles of AA on disk at time t during third stage [mol] and $\bar{M}$ = moles of AA per mean-sized aggregate [mol/aggregate]. Combining eqs 15 and 16 results in an expression for the rate of aggregate desorption during the third stage

$$\frac{d\hat{M}_3}{dt} = -\hat{k}\hat{M}_3 \qquad t_0 < t < \infty \tag{17}$$

The solution to eq 17 is

$$\hat{M}_3(t) = \hat{M}_3(t_0)\exp[-\hat{k}(t - t_0)] \tag{18}$$

A mass balance of the contents of the cleaning solution can be used to relate the time rate of change of the moles of AA on the disk and time rate of change of the moles of AA in solution during the third stage

$$\frac{dM_3}{dt} = -\frac{d\hat{M}_3}{dt} \tag{19}$$

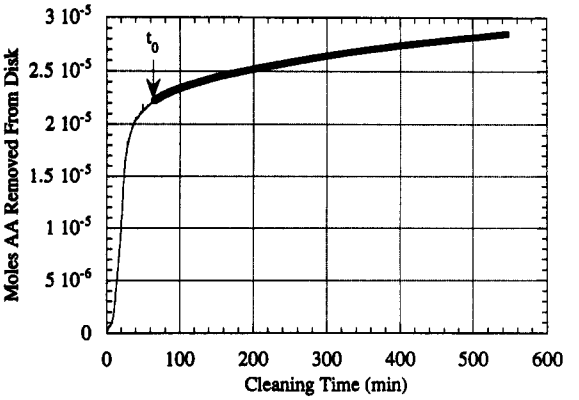

Figure 8. Typical agreement, theory and experiment: third stage cleaning.

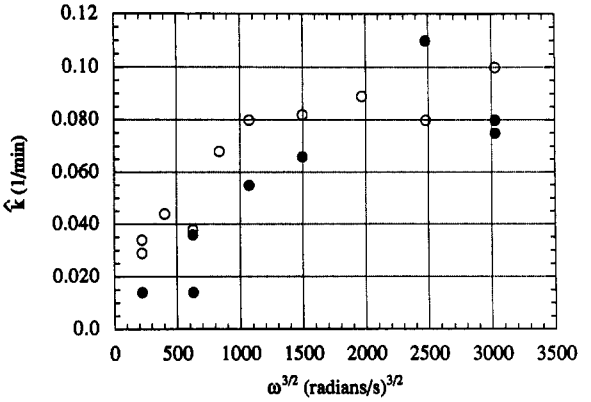

Figure 9. Evaluation of shear-controlled cleaning during third cleaning stage: 4.1×10^{-3} M $C_{12}E_5$, 24 °C (○, disks with 1 AA/IPA coat; ●, disks with 3 AA/IPA coats).

where M_3 = moles of AA in solution during third stage. Integration of eq 19 results in

$$M_3(t) - M_3(t_0) = \hat{M}_3(t_0) - \hat{M}_3(t) \tag{20}$$

Finally, the relationship between the moles AA in solution during the third stage and the moles of AA on the disk during the third stage may be obtained by combining eqs 18 and 20

$$M_3(t) = M_3(t_0) + \hat{M}_3(t_0)[1 - \exp[-\hat{k}(t - t_0)]] \tag{21}$$

Equation 21 was used to fit the third stage data. The values of t_0 and $M_3(t_0)$ were evaluated from the cleaning data as described above and illustrated in Figure 1. The values of the parameters $M_3(t_0)$ and $\hat{k}$ were found by a two-variable least squares minimization of the difference between eq 21 and the experimental data. Figure 8 presents a typical curve-fitting result.

In Figures 9, 10, and 11, the values of $\hat{k}$ obtained from fits of eq 21 to the experimental data are shown as a function of $\omega^{3/2}$, for experiments conducted with 4.1×10^{-3}, 1×10^{-3}, and 6×10^{-5} M $C_{12}E_5$, respectively. Cleaning data for disks with one and three AA/IPA coatings were used to evaluate this parameter. It should be noted that, as the value of the shear stress increases, there is a monotonic increase in the value of the desorption constant, and the value of the desorption constant goes to zero when the shear stress goes to zero. This is consistent with the concept that shear-driven removal of aggregates directly from the FR-4 surface occurs during the third stage.

As can be seen in Figures 9–11, there is no effect of the initial film thickness on the desorption constants

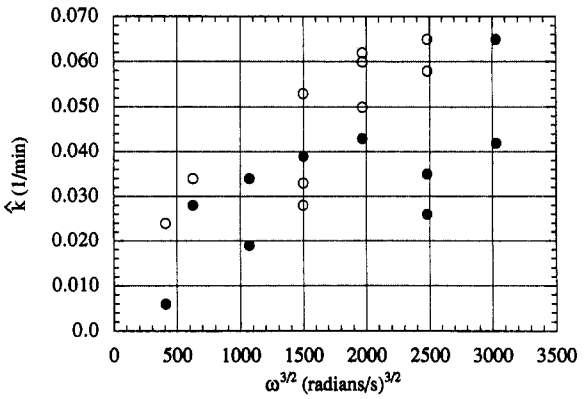

Figure 10. Evaluation of shear-controlled cleaning during third cleaning stage: 1×10^{-3} M $C_{12}E_5$, 24 °C (○, disks with 1 AA/IPA coat; ●, disks with 3 AA/IPA coats).

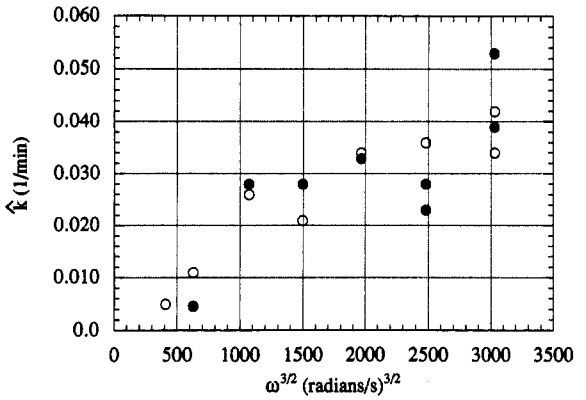

Figure 11. Evaluation of shear-controlled cleaning during third cleaning stage: 6×10^{-5} M $C_{12}E_5$, 24 °C (○, disks with 1 AA/IPA coat; ●, disks with 3 AA/IPA coats).

evaluated for the third stage. Previously, it was stated that the removal of the residual AA "islands" directly from the FR-4 should be independent of the mass of film initially present on the disk, and this is confirmed. Next, as the concentration of surfactant in solution increases, the value of the third stage desorption constant increases. This is thought to be due to the ability of micelles to facilitate the desorption of AA aggregates from the FR-4 surface by either an emulsification or roll-up mechanism (Beaudoin et al., 1995). Also, the effect of surfactant concentration on the third stage desorption is comparable to that seen in the second stage. For example, in Figure 7, at a value of $\omega^{3/2}$ of nearly 1500, k increases by a factor of nearly 3 when the surfactant concentration increases from 1×10^{-3} to 4.1×10^{-3} M, while at the same value of $\omega^{3/2}$, the change seen between Figures 10 and 9 (1×10^{-3} to 4.1×10^{-3} M) is about a factor of 2. In the analysis of the second stage desorption constants, it was seen that at high values of the shear stress for the 4.1×10^{-3} M data, the relationship between the desorption constant and the shear stress was different than at low values of the shear stress. In Figures 9–11, however, this phenomenon is not seen, as the rate of the cleaning is much lower than that seen during the second stage, so that the time required to measure changes in the AA content of the cleaning solution does not affect the results. During the third stage, a significant portion of the surface area of each aggregate is bound directly to the FR-4 prior to desorption. The presence of this inaccessible area reduces the ability of micelles to enhance aggregate removal, compared to the second stage, and this reduces greatly the cleaning rate.

It should be noted that there is some scatter in the data shown in Figures 9–11. The cleaning observed during the third stage was found to be extremely sensitive to both the smoothness of the FR-4 and the interface where the FR-4 met the Teflon holder. Small bumps, gaps, or other irregularities on these surfaces were reflected in the magnitude of the desorption constants evaluated for the third stage. The values of the desorption constants also were very sensitive to the behavior of the second stage near the second stage–third stage transition. Depending on the size of aggregates being removed during the second stage at the transition point, the desorption constant could be inflated or reduced. Finally, the value of the measured desorption constants was found to vary slightly with the duration of the third stage. As a result, in cases where this stage was terminated prematurely, the value of the desorption constant was affected. While every attempt was made to minimize these sources of error, they could not be eliminated entirely.

Conclusions

Simple theoretical models were applied to the different cleaning stages to allow identification of the important cleaning parameters. In the first stage, the cleaning was modeled as though convective transport to and diffusion of surfactant into the AA/IPA layer controlled the progress of the stage. It was determined that there is a strong correlation between the rates of surfactant transport and penetration and the duration of the first stage. Analysis of the agreement between the model and the experimental data suggested that the shear stress at the surface of the film also affects the duration of the first stage. It is apparent that higher shear rates may allow films with lower surfactant concentrations (higher viscosities) to be removed by the aggregate removal mechanism (second stage), thus decreasing the observed duration of the first stage (value of t_c). The model analysis also revealed that increased concentrations of micelles in the aqueous solution facilitated the transition to the aggregate removal stage (second stage). Micelles may augment the concentration of surfactant monomer in the interfacial region, increasing the driving force for penetration into the organic layer, or the micelles may enhance the rate of desorption of aggregates from the surface, hastening the transition from the first to second stages.

The second and third stages were modeled assuming that shear stresses at the surface of the disks cause aggregates to be pulled from the bulk film (second stage) or from the FR-4 surface (third stage). The rate of film removal in these stages was found to be independent of the amount of AA/IPA film initially present on the disk. Increasing the surfactant concentration in solution increased the aggregate removal rate in both stages, resulting in a corresponding increase in the value of the aggregate desorption constants. The modeling effort revealed that the aggregate removal during the second stage is independent of the amount of AA on the disk, while cleaning during the third stage had a first-order dependence on this quantity. This is due to the fact that a continuous film of AA is present on the disk during the second stage, whereas "islands" of AA surrounded by bare FR-4 are present during the third stage.

Acknowledgment

The authors would like to thank Northern Telecom Co. in Research Triangle Park, NC, for providing FR-4 laminate, and AT&T in Princeton, NJ, and the Digital

equipment Corp. in Augusta, ME, for their assistance in planning this work. Funding for this research was received from the Pollution Prevention Research Center at North Carolina State University and from the National Science Foundation Program for Environmentally Benign Chemical Synthesis and Processing (Grant No. CTS-9216850). The authors also would like to acknowledge Christine Palmer, Stacey Julien, and Rochelle Carlton for their assistance in the laboratory.

Nomenclature

$Bi = k_m\delta/(D_{SA}K)$ = mass transfer Biot number, dimensionless
C = concentration of $C_{12}E_5$ in AA/IPA film, mol/L
C_b = bulk surfactant concentration, mol/L
C_S = interfacial surfactant concentration, mol/L
D = $C_{12}E_5$ monomer diffusion coefficient in aqueous solution, cm^2/s
D_{SA} = diffusion coefficient of $C_{12}E_5$ in AA/IPA film, cm^2/s
K = $C_{12}E_5$ partitioning equilibrium constant, dimensionless
k = second stage desorption rate constant, mol/time
k_i = third stage desorption rate constant for aggregates of size i, 1/time
$\hat{k}$ = mean aggregate desorption rate constant, 1/time
k_m = coefficient for transport of surfactant to disk surface, cm/s
M_2 = moles AA in solution during second stage, mol
M_3 = moles AA in solution during third stage, mol
$\hat{M}_3$ = moles AA on disk during third stage, mol
$\bar{M}$ = moles AA per mean-sized aggregate, mol/aggregate
$\bar{N}$ = mean number of aggregates on disk
N_i = number of aggregates on disk surface of size σ_i
$P(\sigma_i)$ = probability of finding an aggregate of size σ_i
r = radial position on disk surface, cm
R = disk radius, cm
t_0 = time at start of third stage, min
t_c = time at end of first stage, min
$U = C/(KC_b)$ = relative saturation of AA/IPA film, dimensionless
$\langle U \rangle$ = average saturation of AA/IPA film, dimensionless
V_r = radial cleaning fluid velocity at film surface, cm/s
$X = z/\delta$ = dimensionless distance into film, dimensionless
z = film thickness, cm

Greek Symbols

α_n = eigenvalues in solution to eq 3, dimensionless
β = proportionality constant for shear-driven particle removal, mol/shear time
δ = film thickness, cm
$\Theta = tD_{SA}/\delta^2$ = dimensionless time, dimensionless
$\Theta_c = t_cD_{SA}/\delta^2$ = dimensionless time at end of first stage, dimensionless
σ_i = characteristic size aggregates on disk during third stage, cm^3
τ_{rz} = shear stress in axial direction on disk surface, $g/cm\cdot s^2$
$\overline{\tau_{rz}}$ = mean shear stress at film surface, $g/cm\cdot s^2$
μ = viscosity of fluid, g/cm·s
ν = kinematic viscosity of fluid, cm^2/s

Literature Cited

Abramowitz, M.; Segun, I. A. *Handbook of Mathematical Functions with Formulas, Graphs, and Mathematical Tables*; Dover Publications: New York, 1968.
Beaudoin, S. P.; Carbonell, R. G.; Grant, C. S. The Removal of Organic Films from Solid Surfaces Using Aqueous Solutions of Nonionic Surfactant. 1. Experiments. *Ind. Eng. Chem. Res.* **1995**, preceding paper in this issue.
Carroll, B. J. The Kinetics of Solubilization of Nonpolar Oils by Nonionic Surfactant Solutions. *J. Colloid Interface Sci.* **1981**, *79*, 126.
Carroll, B. J.; O'Rourke, G. C.; Ward, J. I. The Kinetics of Solubilization of Single Component Non-Polar Oils by a Non-Ionic Surfactant. *J. Pharm. Pharmacol.* **1982**, *34*, 287.
Cochran, W. G. The Flow Due To A Rotating Disk. *Proc. Cambridge Philos. Soc.* **1934**, *30*, 365.
Geankoplis, C. J. *Transport Processes and Unit Operations*, Prentice Hall: Englewood Cliffs, NJ, 1983.
Levich, B. The Theory of Concentration Polarization. *Acta Physicochim. URSS* **1942**, *XVII*, 257.
Middleman, S. The Effect of Induced Air-Flow on the Spin Coating of Viscous Liquids. *J. Appl. Phys.* **1987**, *62*, 2530.
Shaeiwitz, J. A.; Chan, A. F.-C.; Cussler, E. L.; Evans, D. F. The Mechanism of Solubilization in Detergent Solutions. *J. Colloid Interface Sci.* **1981**, *84*, 47.
Strong, L.; Middleman, S. Lubricant Retention on a Spinning Disk. *AIChE J.* **1989**, *35*, 1753.

Received for review January 3, 1995
Revised manuscript received May 23, 1995
Accepted June 14, 1995[⊗]

IE950015J

[⊗] Abstract published in *Advance ACS Abstracts,* August 15, 1995.